DOI: https://doi.org/10.46354/i3m.2019.iwish.002

EVALUATING KINECT V1 AND V2 FOR CHEST WALL SURFACE SCANNING AND ASSESSMENT

Nahom Kidane[(a)], Mohammad F. Obeid[(b)], Cierra Hall[(c)], Ntiana Sakioti[(d)], Robert E. Kelly[(e)], Frederic D. McKenzie[(f)]

[(a),(c),(d),(f)]Dept. of Computational Modeling and Simulation Engineering, Old Dominion University Norfolk, USA
[(b)]Division of Applied Technology, Shenandoah University, Winchester, USA
[(e)]Pediatric Surgery, Children's Hospital of The King's Daughters and Eastern Virginia Medical School, Norfolk, USA

[(a)]nkidane@odu.edu, [(c)] chll012@odu.edu, [(d)]nsaki001@odu.edu, [(f)] rdmckenz@odu.edu, mobeid@su.edu [(b)]
[(d)] Robert.Kelly@chkd.org

ABSTRACT
Optical scanning has proven to be advantageous to objectively assess the severity of chest wall deformities and the effectiveness of its treatment. By potentially eliminating the need for computed tomography (CT) scanning and superseding manual measurements that are subject to errors, a system that utilizes optical scanning presents great value to patients and practitioners. This work aims to investigate and evaluate the performance of two off-the-shelf optical scanning sensors in the context of their utility and accuracy to measure the severity of chest wall deformities. An in-vitro experiment and a human study are conducted utilizing both sensors to collect data and report the findings.

Keywords: Chest deformities, surface scanning, Kinect sensor

1. INTRODUCTION

Pectus Excavatum (PE) is a chest wall deformity characterized by a depression of the sternum and accounts for nearly 90% of all congenital chest malformations (Williams & Crabbe, 2003). Commonly diagnosed in early adolescence, the severity of the deformation determines a patient's candidacy for surgical (e.g., Nuss procedure (Nuss, Robert E. Kelly, Croitoru, & Katz, 1998)) or conservative nonsurgical treatment (e.g., Vacuum Bell (Haecker, 2011)).

Severity, as well as treatment progress, is commonly determined by rudimentary techniques such as simple linear measurements using dowel-shaped rulers (Brigato, Campos, Jatene, Moreira, & Rebeis, 2008) or through expert evaluation of indices (Haller Index (Haller, Kramer, & Lietman, 1987) or Correction Index (Peter et al., 2011)) calculated from the patient's computerized tomography (CT) image. However, CT is expensive and results in extensive exposure to harmful ionizing radiation, while manual techniques can be inaccurate and inherently subjective.

Recent hardware and software advancements in 3D imaging have led to the rise of low-cost, portable, and mass-market 3-dimensional scanning devices. These tools capture the surface geometry of objects and have shown great potential in recording, quantifying, and tracking chest wall deformity (Glinkowski et al., 2009; Poncet et al., 2007).

To mitigate misdiagnoses and monitor PE treatment, we developed an imaging system that uses Microsoft Kinect Version 1 (Figure 1-a) to obtain surface scans of the pectus deformity and provide informative metrics of the target area (Kelly et al., 2018). Our technique was verified to measure distances from the probe accurately and was found to be sufficient for the application (Obeid, Kidane, et al., 2016; Obeid, Obermeyer, Kidane, Kelly, & McKenzie, 2016; Zeng et al., 2016). Nonetheless, scanning technology is evolving rapidly, raising the challenge of selecting a suitable scanning device that can further enhance the usability of our systems.

This paper aims to compare two versions of Microsoft Kinect (V1 and V2), in the application of evaluating the severity and treatment of chest wall deformity. A three-fold experiment was conducted involving four different types of targets to be scanned: (1) a flat white surface, (2) male and female mannequin torsos, (3) a 3D-printed pectus phantom, (4) and nineteen healthy individuals. The results are validated against the ground truth (GT) of anatomical landmark distances recorded with Vernier caliper and a tape measure, as well as, in the flat test object case, mathematical plane surface. Other comparative studies (F. Redaelli, Gonizzi Barsanti, Fraschini, Biffi, & Colombo, 2018; Pöhlmann, Harkness, Taylor, & Astley, 2016; Sarbolandi, Lefloch, & Kolb, 2015) have explored the characteristics and differences between these devices for computer vision and healthcare applications (e.g., Orthopedic (Pöhlmann et al., 2016)), but to the best of our knowledge, no study has been conducted assessing the accuracy and application of these two sensors for pediatric chest wall deformity.

This paper is organized as follows: Section II will summarize background information on the sensors, while Section III will present the methods for comparison and data collection. Section IV will highlight experimental results and subsequent sensor selection for the relevant work. Finally, Section V will discuss conclusory remarks and propose potential future work.

2. BACKGROUND

The first-generation Kinect (V1) has two cameras colored RGB (Red, Green, Blue) and a monochrome NIR Near-infrared camera, as well as a NIR projector with a laser diode of 850 wavelengths (F. Redaelli et al., 2018). Depth determination is conducted based on structured light. The device starts by releasing infrared light onto an object which is then broken into a pattern by a diffraction grating. Patterns are sectionalized into neighborhoods and analyzed. Depending on the object's distance from the sensor, the light becomes distorted, and a 3D triangulation technique is used to compute the depth of the object (Pöhlmann et al., 2016). However, the device may produce inaccurate data in the event an object with challenging geometry is scanned, due to the disruption inflicted upon the neighborhood, making it difficult to determine between distorted and undistorted patterns.

The second generation of Kinect (V2) is composed of a 512 x 414 depth image sensor, where each 10 µm x 10 µm pixel incorporates a Time-Of-Flight (TOF) detector that operates using the Quantum Efficiency Modulation (F. Redaelli et al., 2018; Wasenmüller & Stricker, 2017). Depth evaluation of a Kinect V2 is determined through a TOF technology. The device measures the total time it takes for infrared light to make a round trip journey from the device to the object and back. The phase shift is analyzed by comparing the incoming signal to four phase-shifted control signals (Pöhlmann et al., 2016). An object's reflectiveness may skew data showing higher depth values due to the noise presented into the depth measurement.

(a) (b)

Figure 1: Microsoft Kinect (a) V1 and (b) V2.

Table 1: Comparison of Kinect sensors for surface scanning.

	Kinect V1	**Kinect V2**
Release	2010	2013
Technology	Struct. light	Time-of-flight
Depth image (pxls)	320 x 240	512 x 424
FOV (degrees)	54 x 43	70 x 60
Range (m)	Up to 6	Up to 4.5

3. METHODOLOGY

3.1. Experiments

Experiment A: The purpose of this experiment is to determine the spatial uncertainty for different operating distances. Each depth sample collected by the sensor is comprised of (1) actual measured values, (2) unavoidable random error due to environmental conditions such as thermal or electronic noise, and (3) a systematic error due to device miscalibration or incorrect use (Guidi, Gonizzi Barsanti, & Micoli, 2016). The precision of the sensor is limited by the random error, which can only be statistically modeled and noted as the device's intrinsic limitation. The accuracy, on the other hand, is influenced by the systematic error, which is difficult to detect but can be minimized with proper calibration. The combinations of these two errors represent global spatial uncertainty.

Following a similar approach used by (F. Redaelli et al., 2018; Guidi et al., 2016), global spatial uncertainty for the two sensors in this study was evaluated by scanning a flat test object (Figure 2-a) and measuring the deviation of the scanned reference surface from an ideal plane. For each flat surface scan, acquired at four different operating distances, we estimated the deviation of the observed 3D surface against a best-fitting mathematical plane model. Additionally, a low-pass filter was used to remove the high-frequency random error component and highlight systematic distortion.

Experiment B: In this experiment, we evaluated the dimensional accuracy of the sensors by comparing known landmark distances of selected rigid physical objects against their virtual counterparts (3D models collected by scanning the objects with the two sensors). For this purpose, we used plastic mannequins and a 3D printed PE replica with fiducial markups (Figure 2b-d). The geometric details on the mannequins mimic the human body, albeit in a rigid way; whereas the 3D-printed PE replicated the anticipated patient morphology. Fiducial markers were placed on the belly button/navel (N), sternal notch (S), nipples (Rp & Lp), center chest line, and upper chest area. However, for ground truth, only the "sternal notch to navel" (S-N) and "right nipple to left nipple" (Rp-Lp) linear (Euclidean) distance were recorded using a Vernier caliper. The same distances were digitally measured on the acquired 3D surface using a virtual ruler (Figure 6).

Experiment C: The final experiment investigated the accuracy of the two sensors to capture dimensions on human subjects. In a clinical setting, landmarks show relative displacements due to the patient's change in posture and skin or soft tissue movement due to breathing. In a fashion similar to the test conducted in experiment B, a trained nurse placed fiducial markers on the navel, sternal notch, and nipples. For ground truth, "sternal notch to navel" (S-N) and nipple (Rp-Lp) distances were measured manually on the subjects. However, in this case, surface distance instead of linear

distance was recorded using a flexible tape measure. The mean deviation between the digital (Figure 8) and hand-measured values of the distances quantifies the dimensional accuracy used to compare the two sensors.

3.2. Test Objects

The study involved four different test objects. Similar to (F. Redaelli et al., 2018; Guidi et al., 2016), a float glass was selected as a flat reference surface due to the smooth and close approximation of a theoretical plane. The glass (Figure 2-a) had a dimension of 58 cm x 48 cm and a thickness of 0.05 cm. It was painted matte white to be sensed by the devices, and four markers were placed to create a region of interest.

In addition to the object described above, three other objects emulating human chest profile were used to evaluate dimensional accuracy. The first two consisted of male and female plastic mannequins with fiducial markups (Figures 2-b and 2-c). The third object was a physical replica of real PE patient obtained by scanning a patient before undergoing the Nuss procedure surgery and 3D-printing the model (Figure 2-d). The PE phantom had dimensions of 27 x 21 cm with the deepest point of deformity at 25 mm.

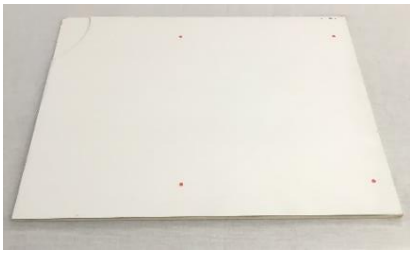

(a)

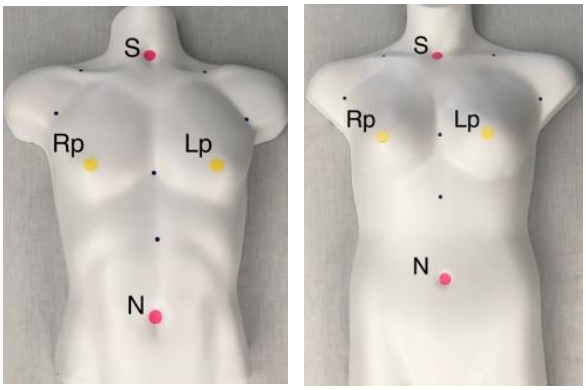

(b) (c)

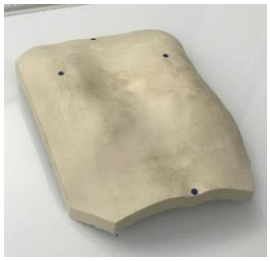

(d)

Figure 2: Objects used for experiment: (a) glass, (b) male mannequin, and (c) female mannequin, and (d) 3D-printed pectus chest.

3.3. Subjects

Nineteen healthy individuals (all males, age: 11 ± 2 years, height: 155. ± 14.7 in.) with no chest deformity participated in this study. The Eastern Virginia Medical School ethics committee approved the study (EVMS IRB# 14-10-EX-0214), and all subjects signed consent forms before data collection (Figure 3-b).

3.4. Data Acquisition

3D surfaces were acquired using ReconstructMe (Heindl & Kopf., 2012) for Kinect V1, and Microsoft Kinect Fusion SDK (Microsoft, 2014) for Kinect V2. For ReconstructMe, the volume bounding box was fixed to 1 x 1 x 1 m at an offset of 0.1 m – 0.50 m from the camera. Similarly, for Fusion SDK, volume voxels per meter were set to 768 with the voxel resolution of 512 x 512 x 512. The depth threshold was fixed at 0.5 m in front of the camera with a bounding box size varying from 1.00 m ~ 2.0 m in order to fully capture the torso.

Scans were collected utilizing a supine test subject/object position/posture. The sensors were fixed on a curved platform which was mounted on a movable overhead frame, as shown in Figure 3, allowing for stable arc motion.

The test objects were scanned at four different distances from the sensors: 0.7 m, 0.8 m, 0.9 m, and 1.0 m. It is important to note that the objects were placed on the table with the sensor height adjustment occurring by sliding the overhead platform with increments of 0.1 m (Figure 3-a). All four items were scanned using the two sensors individually before moving to scan at the next height. Both snapshot (sensor is stationary) and continuous (moving the sensor on the curved frame) scanning approaches were used to capture full sides of the figure. The data acquisition was stopped after 5 seconds for snapshot and 30 seconds for continuous scanning.

Unlike the test objects, the human subjects were scanned with the sensor mounted at a distance of 0.9 m from the subject. The camera was rotating 130° around the subject to capture the front and sides of the torso. Both Kinect V1 and V2 were running simultaneously for comparison (Figure 3-b).

3.5. Data Processing

After the scanning procedure, raw 3D data was saved as a colored polygon (.ply format) mesh file. All further processing steps are done on the opensource MeshLab (Cignoni et al., 2008), and GOM inspect (GOM, 2013) software applications. The mesh data is used as provided by the sensors with minor pre-processing such as removal of artifact points or undesired background objects. For Kinect V2, the 3D model was scaled by a factor 1000 to convert to millimeter units.

The flat glass surface was cropped into 20 x 20 cm area, and the Taubin filter (λ = 0.95, μ = -0.98 with 50 iterations) was also utilized in MeshLab to remove high-frequency components from the global error and highlight systematic error (Taubin, 1995).

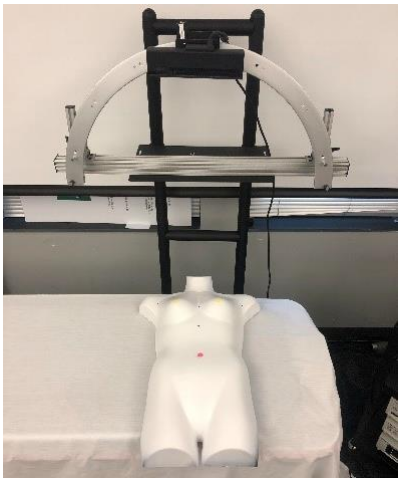

(a)

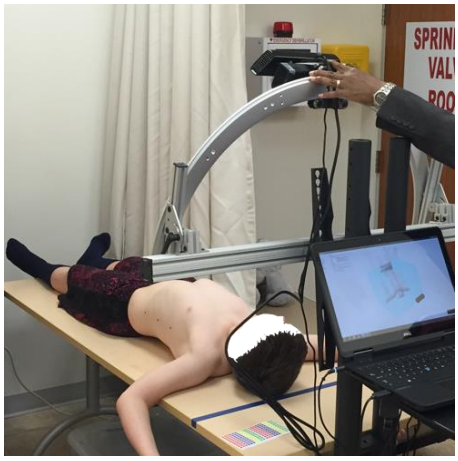

(b)

Figure 3: the scanning procedure: (a) scanning a mannequin and (b) scanning a healthy subject.

4. RESULTS AND DISCUSSION

4.1. Experiment A

Spatial uncertainty is reported as the standard deviation (SD) of the 3D surface from the fitted mathematical plane model. Table 2 and Figure 4 illustrate the global uncertainty/error (σ_u) for both sensors. Similar to (F. Redaelli et al., 2018; Guidi et al., 2016) systematic error (σ_s) is deduced by applying Taubin filter. Lower values indicate better device performance. The first-generation Kinect (V1) had a higher global error (SD ≤ 1.5 mm) for the tested sensor range. The error did not exceed 0.5 mm for Kinect V2, and it remained stable over the operating distances. Trends were within the expected interval and consistent with other comparative studies (F. Redaelli et al., 2018; Guidi et al., 2016; Pöhlmann et al., 2016).

Table 2: SD of the point-to-plane distance for the float glass test object at different sensor distance

	Global (σ_u) and Systematic (σ_s) Errors [mm]							
	0.7 m		0.8 m		0.9 m		1.0 m	
Device	σ_u	σ_s	σ_u	σ_s	σ_u	σ_s	σ_u	σ_s
V1	1.10	1.07	1.25	1.21	1.45	1.39	1.48	1.44
V2	0.41	0.41	0.44	0.39	0.39	0.34	0.34	0.31

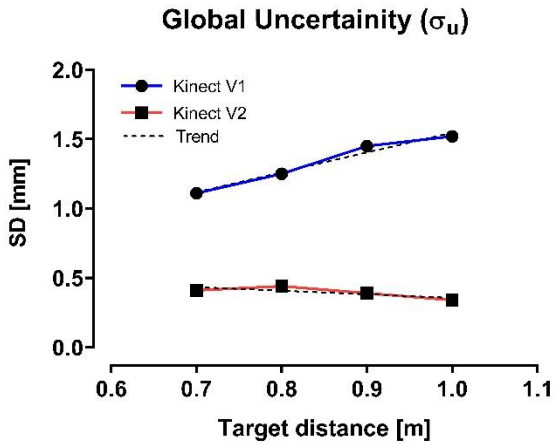

Figure 4: Standard deviation of measurement error to fitted plane at different sensor distances.

Compared to Redaelli et.al (F. Redaelli et al., 2018), we observe lower error values for both sensors, which may be explained by the different methods used to fit the ideal plane; we used a best-fit method while they used Iterative Closest Point (ICP). Figure 5 shows the point to plane deviation at sensor distance 0.8 m. For Kinect V1, approximately 45% of the observed deviation was below 1.0 mm, and 0.82% were within 2 mm. For Kinect V2, 80% of observed deviation was below 0.5 mm and 97% was under 1.0 mm. This result is similar to one reported by (Pöhlmann et al., 2016).

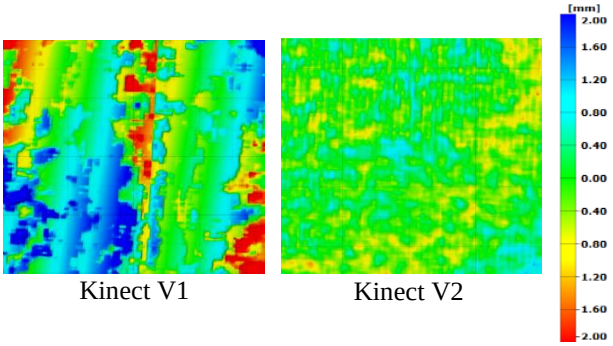

Kinect V1 Kinect V2

Figure 5: Color-mapped point-to-plane deviation of the 3D cloud from the fitted ideal plane for data collected with both sensors at 0.8 m operating distance.

4.2. Experiment B

As previously mentioned, the ground truth is the caliper/tape manual measurement. Therefore, a deviation from that measurement was computed for all scanned objects. Figure 6 shows an example of a virtual measurement obtained for the male mannequin object. Figure 7 shows the dimensional accuracy plot for all 3 objects, for both S-N and Rp-Lp distances, and for both sensors; it presents the millimeter difference box plot.
Kinect V2 showed better results for both Rp-Lp (right nipple to left nipple) and S-N (sternal notch to navel) distances than V1. A one-sample t-test was conducted to determine whether the virtual measurements were different from the ground truth, comparing the mean error score to zero. All virtual measurements passed

Shapiro-Wilk's normality test ($p > 0.05$). The S-N distance deviation of the female mannequin (1.5, 95% CI, -3.19 to 6.18) and PE phantom (-1.38, 95% CI, -3.6 to 0.89) was not significantly different from zero. The Rp-Lp distance deviation for the male mannequin (0.75, 95% CI, -.049 to 1.98) and PE phantom (-0.87, 95% CI, -2.19 to 0.35) was also found to be not statistically significant. However, on Kinect V1, only mean deviation from the female mannequin was found to be not significant (S-N = 1.5, 95% CI, -3.19 to 6.18 and Rp-Lp = -1.38, 95% CI, -3.6 to 0.89); whereas all other measured values were found to be significantly larger or smaller ($p < 0.05$) than measured ground truth.

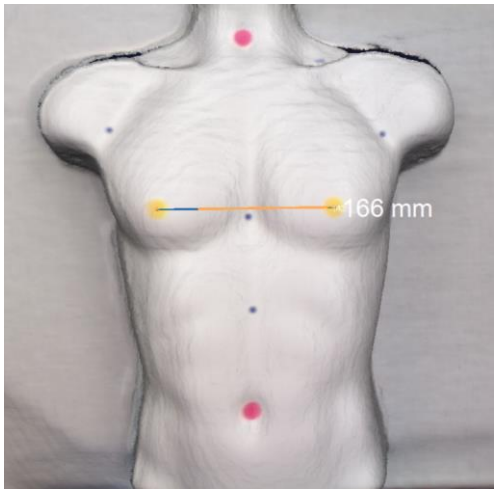

Figure 6: Illustration of obtaining virtual measurements (in this case for object: male mannequin).

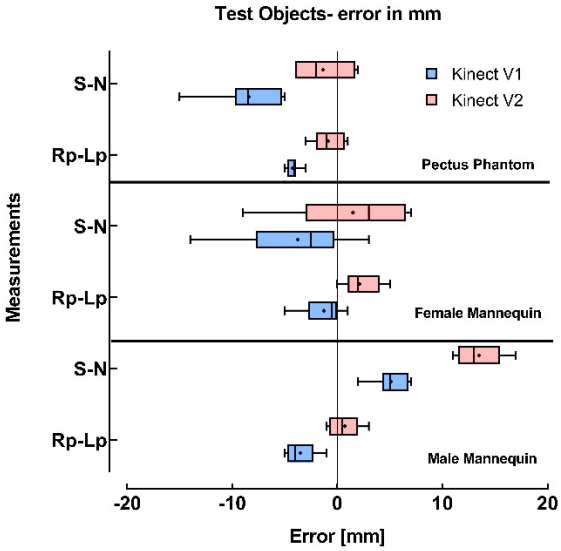

Figure 7: Test object millimeter difference error box plot.

4.3. Experiment C

The purpose of the final experiment was to validate the sensors in a clinical setting. We evaluate the hypothesis that distances measured from Kinect V1 and Kinect V2 data are equivalent to the real measurements obtained from a human participant's chest surface using a tape measure. Figure 8 shows an example of a virtual measurement for one of the participants.

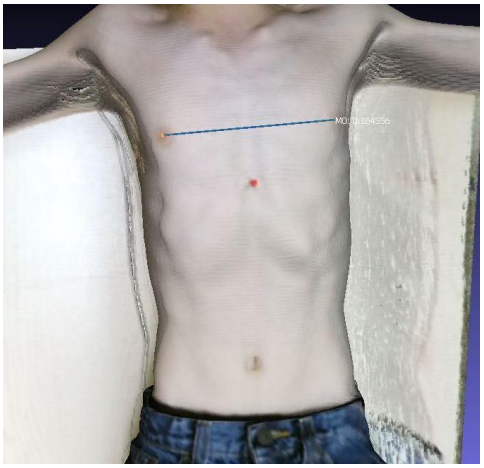

Figure 8: Illustration of obtaining virtual measurements for a real healthy subject.

The equivalency analysis assesses whether mean variations are small enough to be deemed acceptable. The discrepancy (Δ) values for Rp-Lp and S-N were selected to be 1.4 cm and 4.5 cm, respectively. We derive these values from the average anthropometric diameter of the nipple and navel (Kawale et al., 2013; Tanini & Lo Russo, 2018).

The nipple diameter (areola) for males ranges from 0.5 - 1.0 cm, with a mean value of 0.7 cm (Tanini & Lo Russo, 2018). Therefore, $\Delta = 1.4$ is acceptable as it is equivalent to 2x an average nipple diameter, representing negligible variation when using different measurement techniques (e.g., inside or outside the nipple-nipple distance).

Similarly, the average navel diameter varies from 1.5 to 2.5 cm, the average sternal notch width is 5 cm, and the average sternal notch to navel distance is 40-45 cm (Kawale et al., 2013). Therefore, we choose Δ to be 4.5 cm, which is 10% S-N distance. Figure 9 shows the 90% confidence interval and the zone of indifference.

Digitally measured Rp-Lp distances showed acceptable agreement with the manual measurements. Both sensors were found to be equivalent, with the 90% CI falling inside the indifference zone. It should be noted that for a two-sided t-test, only actual-vs.-Kinect V2 outcome (6.21, 95% CI, -0.02 to 12.61) was not statistically different from zero ($p = 0.58$). However, for S-N measurement, all actual-vs.-Kinect groups were statistically different from zero and not equivalent.

4.4. Discussion

Spatial uncertainty was evaluated by scanning a flat test object at a range of 0.7 m - 1.0 m and measuring deviation to a fitted mathematical plane model. This range is suitable for clinical PE chest scanning application. Our results showed lower global uncertainty for Kinect V2 with 97% of deviation below 1 mm; the error remained stable for the operating distances. The device performance obtained from the simple flat surface is only a preliminary indication of the sensor's performance and may vary in a real clinical setting.

When evaluating linear dimensional accuracy using rigid objects, Kinect V2 outperformed V1, but both devices exhibited errors for the larger linear distance (S-N).
Dimensional accuracy was also assessed in a clinical setting. Although both sensors showed acceptable agreement with manual measurements for the Rp-Lp distance, Kinect V2, in particular, showed an error not statistically different from zero ($p = 0.058$). However, all digital measurements performed worse for S-N distance in human subjects. A plausible explanation for the relatively large error maybe the size of the anatomical landmarks. Higher variability is expected when manually annotating large anatomical landmarks such as the sternal notch as it allows more room for inconsistency and human error. Furthermore, the digitally defined surface path between the two points may be different from the manual measurement.

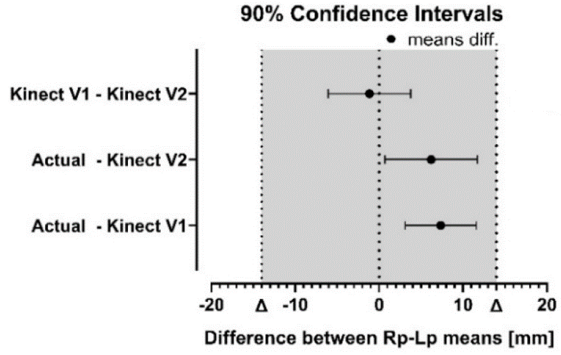

(a)

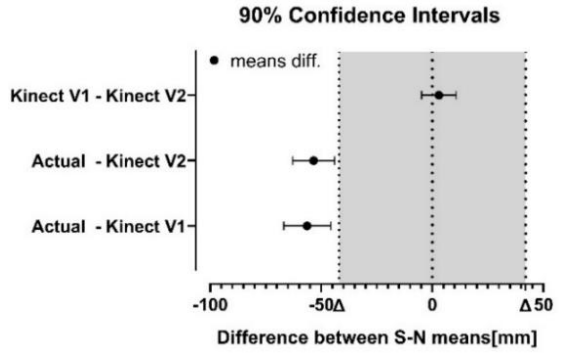

(b)

Figure 9: 90% confidence interval and zone of indifference for (a) Rp-Lp means and (b) S-N means.

5. CONCLUSION

Recent advancements in imaging have led to the rise of low-cost 3-dimensional scanning devices. While the technology is evolving rapidly, a challenge of selecting a suitable device for medical applications rises.
This paper compares two generations of Microsoft Kinect (V1 &V2) scanning sensors that use two different technologies (structure light and time-of-flight) in the context of assessing chest wall deformities. This was done by conducting a 3-fold experiment to investigate the spatial uncertainty as well as the linear dimensional accuracy of the two devices. Kinect V2 showed a level of accuracy that exceeded that of V1 and allows the capturing of small anatomical features in a clinical setting. For assessing chest wall deformities such as pectus excavatum, this study shows that V2 can provide a more reliable evaluation of the condition (than V1) and can better inform on treatment progress.

ACKNOWLEDGMENTS

The authors gratefully acknowledge the Children's Surgical Specialty Group and Children's Hospital of The King's Daughters for their generous support. The authors also acknowledge the assistance of Mrs. Kristina Laws.

REFERENCES

Brigato, R. R., Campos, J. R. M., Jatene, F. B., Moreira, L. F. P., & Rebeis, E. B. (2008). Pectus excavatum: evaluation of Nuss technique by objective methods. *Interactive CardioVasc Thoracic Surgery, 7*(6), 1084-1088.

Cignoni, P., Callieri, M., Corsini, M., Dellepiane, M., Ganovelli, F., & Ranzuglia, G. (2008). *Meshlab: an open-source mesh processing tool.* Paper presented at the Eurographics Italian chapter conference.

F. Redaelli, D., Gonizzi Barsanti, S., Fraschini, P., Biffi, E., & Colombo, G. (2018). Low-cost 3D devices and laser scanners comparison for the application in orthopedic centres. *ISPRS - International Archives of the Photogrammetry, Remote Sensing and Spatial Information Sciences, XLII-2,* 953-960. doi:10.5194/isprs-archives-XLII-2-953-2018

Glinkowski, W., Sitnik, R., Witkowski, M., Kocon, H., Bolewicki, P., & Gorecki, A. (2009). Method of pectus excavatum measurement based on structured light technique. *Journal of biomedical optics, 14*(4), 044041. doi:10.1117/1.3210782

GOM. (2013). GOM Inspect. Retrieved from https://www.gom.com/3d-software/gom-inspect.html

Guidi, G., Gonizzi Barsanti, S., & Micoli, L. L. (2016). 3D capturing performances of low-cost range sensors for mass-market applications. *International Archives of the Photogrammetry, Remote Sensing and Spatial Information Sciences, XLI-B5*, 33-40.

Haecker, F.-M. (2011). The vacuum bell for conservative treatment of pectus excavatum: the Basle experience. *Pediatric Surgery International, 27*(6), 623-627.

Haller, J. A., Jr., Kramer, S. S., & Lietman, S. A. (1987). Use of CT scans in selection of patients for pectus excavatum surgery: a preliminary report. *J Pediatr Surg, 22*(10), 904-906. doi:S0022346887000277 [pii]

Heindl, C., & Kopf., C. (2012). ReconstructMe. Retrieved from http://reconstructme.net/

Kawale, M. M., Reece, G. P., Crosby, M. A., Beahm, E. K., Fingeret, M. C., Markey, M. K., & Merchant, F. A. (2013). Automated Identification of Fiducial Points on 3D Torso Images. *Biomedical engineering and computational biology, 5*, 57-68. doi:10.4137/BECB.S11800

Kelly, R. E., Jr., Obermeyer, R. J., Kuhn, M. A., Frantz, F. W., Obeid, M. F., Kidane, N., & McKenzie, F. D. (2018). Use of an Optical Scanning Device to Monitor the Progress of Noninvasive Treatments for Chest Wall Deformity: A Pilot Study. *The Korean journal of thoracic and cardiovascular surgery, 51*(6), 390-394. doi:10.5090/kjtcs.2018.51.6.390

Microsoft. (2014). Kinect -Windows app development. Retrieved from https://developer.microsoft.com/en-us/windows/kinect

Nuss, D., Robert E. Kelly, J., Croitoru, D. P., & Katz, M. E. (1998). A 10-year review of a minimally invasive technique for the correction of pectus excavatum. *Journal of Pediatric Surgery, 33*(4), 545-552.

Obeid, M. F., Kidane, N., Rechowicz, K. J., Chemlal, S., Kelly, R. E., & McKenzie, F. D. (2016). Validation of an objective assessment instrument for non-surgical treatments of chest wall deformities. *Studies in Health Technology and Informatics, Medicine Meets Virtual Reality 22, 220*, 273 - 280.

Obeid, M. F., Obermeyer, R., Kidane, N., Kelly, R. E., & McKenzie, F. D. (2016). *Investigating the fidelity of an improvement-assessment tool after one vacuum bell treatment session.* Paper presented at the Proceedings of the Summer Computer Simulation Conference (SCSC '16), Montreal, Quebec, Canada.

Peter, S. D. S., Juang, D., Garey, C. L., Laituri, C. A., Ostlie, D. J., Sharp, R. J., & Snyder, C. L. (2011). A novel measure for pectus excavatum: the correction index. *Journal of Pediatric Surgery, 46*(12), 2270-2273.

Pöhlmann, S. T. L., Harkness, E. F., Taylor, C. J., & Astley, S. M. (2016). Evaluation of Kinect 3D Sensor for Healthcare Imaging. *Journal of Medical and Biological Engineering, 36*(6), 857–870.

Poncet, P., Kravarusic, D., Richart, T., Evison, R., Ronsky, J. L., Alassiri, A., & Sigalet, D. (2007). Clinical impact of optical imaging with 3-D reconstruction of torso topography in common anterior chest wall anomalies. *Journal of Pediatric Surgery, 42*(5), 898-903. doi:10.1016/j.jpedsurg.2006.12.070

Sarbolandi, H., Lefloch, D., & Kolb, A. (2015). Kinect range sensing: Structured-light versus Time-of-Flight Kinect. *Computer Vision and Image Understanding, 139*, 1-20.

Tanini, S., & Lo Russo, G. (2018). Shape, Position and Dimension of the Nipple Areola Complex in the Ideal Male Chest: A Quick and Simple Operating Room Technique. *Aesthetic Plast Surg, 42*(4), 951-957.

Taubin, G. (1995). *A signal processing approach to fair surface design.* Paper presented at the Proceedings of the 22nd annual conference on Computer graphics and interactive techniques.

Wasenmüller, O., & Stricker, D. (2017, 2017//). *Comparison of Kinect V1 and V2 Depth Images in Terms of Accuracy and Precision.* Paper presented at the Computer Vision – ACCV 2016 Workshops, Cham.

Williams, A. M., & Crabbe, D. C. G. (2003). Pectus deformities of the anterior chest wall. *Paediatric Respiratory Reviews, 4*(3), 237-242.

Zeng, Q., Kidane, N., Obeid, M. F., Chen, C., Shen, R., Kelly, R. E., & McKenzie, F. D. (2016). Utilizing Pre- and Postoperative CT to Validate an Instrument for Quantifying Pectus Excavatum Severity. In Z. L., S. X., & W. Y. (Eds.), *Theory, Methodology, Tools and Applications for Modeling and Simulation of Complex Systems* (Vol. 645): Springer, Singapore.

AUTHORS BIOGRAPHY

Nahom Kidane, M.S., is a Ph.D. candidate and an Adjunct Professor at Old Dominion University's Computational Modeling and Simulation Engineering Department. He received his BS degree in Electrical Engineering from Jimma University, Jimma, Ethiopia and his MS degree in Modeling and Simulation Engineering from Old Dominion University, Norfolk, Virginia. His main areas of research are medical simulation, 3D deep learning, augmented reality, and scientific visualization.

Mohammad F. Obeid, Ph.D. is an Assistant Professor at Shenandoah University's Division of Applied Technology. Previously, he served as an Instructor and a researcher at Old Dominion University's Computational Modeling and Simulation Engineering Department. He received his BS degree in Industrial Engineering from the German Jordanian University in Amman, Jordan in 2011; his MS degree in Modeling and Simulation Engineering from Old Dominion University in Norfolk, Virginia in 2013; and his PhD degree in Modeling and Simulation Engineering from Old Dominion University in 2017. Currently, he is involved with research projects in virtual/augmented reality applications for simulated, surgical, and computer assisted interventions. His research interests include medical modeling and simulation, surgery simulation, biomedical engineering, and extended reality applications.

Cierra Hall is a post-baccalaureate student at Old Dominion University's Computational Modeling and Simulation Engineering Department. She received her B.S. in Paralegal Studies at the University of Richmond, Richmond, Virginia. She currently works as an intern in the field of machine learning and parallel computing on autonomous aerial drones. Her research interests include big data analysis, machine learning, parallel computing, and autonomous systems. Cierra lives in Chesapeake, Virginia with her husband Petty Officer First Class Richard Davis III and their two Labrador Retrievers.

Ntiana Sakioti is a Graduate Student and Teaching Assistant at Old Dominion University's Computational Modeling and Simulation Engineering Department. She received her BS degrees in Electrical Engineering and

Computer Engineering from Old Dominion University, Norfolk, Virginia. Her research interests include autonomous systems in particular autonomous vehicles, simulation-based testing, and behavioral modeling.

Robert E. Kelly, Jr., M.D. received his medical degree from The Johns Hopkins University in 1985. He completed his General Surgery Residency at Vanderbilt University School of Medicine and his Pediatric Surgery Fellowship at Children's Hospital of Buffalo. Dr. Kelly also completed an ECMO and Surgical Research Fellowship at UCLA School of Medicine. In 1994, Dr. Kelly joined Children's Surgical Specialty Group-Pediatric Surgery and has been the Chairman of the Department of Surgery at Children's Hospital of The King's Daughters since 1998. He is also a Professor of Clinical Surgery and Pediatrics in the Department of Surgery at Eastern Virginia Medical School. Dr. Kelly lives in Norfolk, Virginia with his wife, Dr. Cynthia Kelly, and their three children.

Frederic (Rick) D. McKenzie, Ph.D. was born in Kingston, Jamaica. Dr. McKenzie has a B.S. in engineering, M.S. in computer engineering, and a Ph.D. in computer engineering all from the University of Central Florida in Orlando, Florida U.S.A. Currently, he is the Department Chair in the Computational Modeling and Simulation Engineering (CMSE) Dept. and a joint faculty member in the Department of Electrical and Computer Engineering (ECE) at Old Dominion University in Norfolk, Virginia U.S.A. In addition, Dr. McKenzie is the co-director of the Medical Imaging, Diagnosis, and Analysis (MIDA) Laboratory, Adjunct Associate Professor of Eastern Virginia Medical School (EVMS) in the School of Health Professions, and Graduate Faculty Scholar at University of Central Florida (UCF) in the School of Electrical Engineering and Computer Science. Before coming to Old Dominion University, he spent 6 years in the simulation industry at Science Applications International Corporation (SAIC) as a senior scientist. Dr. McKenzie's research has been in medical modeling and simulation, human behavior representation, and simulation architectures often focusing on aspects of scientific visualization and virtual reality.